44th AIAA Plasmadynamics and Lasers Conference
26-29 June 2013, San Diego, CA
AIAA-2013-3132

# The Improvement of the Aero-Optical Environment of a Hemisphere-on-Cylinder Turret using Vortex Generators

N. De Lucca[1], S. Gordeyev[2] and E. Jumper [3]
*University of Notre Dame, Notre Dame, Indiana 46545, USA*

**Aero-optical mitigation effect of a passive flow control device consisted of a pair of delta-wing vortex generators placed on both sides near a hemisphere-on-cylinder turret was experimentally studied in-flight aboard the Airborne Aero-Optics Laboratory (AAOL) at different subsonic speeds. The optical environment was characterized with a 2D high speed Shack-Hartmann wavefront sensor. Wavefronts were acquired at a variety of viewing angles for both flat and conformal window turrets. Flight data were compared to both tunnel data and CFD simulations to give insight into how vortex generators alter the flow field around the turret for potential improvement of the aero-optical performance. In CFD simulations the vortex generators were shown to move the necklace vortex away from the turret and horn vortices were modified. Vortical generators were shown to reduce $OPD_{RMS}$ for a range of back-looking viewing angles**.

## 1. Introduction

The hemisphere-on-cylinder turret is a common projection platform for directed energy systems as it provides simple means of maximizing the field-of-regard of the system. For turrets mounted on aircraft moving at subsonic or faster speeds, however, the compressible nature of the flow and the highly-complex three-dimensional flow field around the turret introduces aberrations into the beam which limit the potential field-of-regard of the directed energy system [1]. In recent years, the Airborne Aero-Optics Laboratory platform has been used to extensively map out the aero-optical performance of several turret configurations, including a flat window [2], a conformal window [3] and a hemisphere only [4]. Additional work has been done by other groups to investigate flow features of turret configurations using CFD [5,6,7,8].

As shown in Figure 1, left, the upstream portion of the flow field around the turret is relatively benign; the curvature of the turret induces a favorable pressure gradient that keeps the flow attached. The curvature of the downstream portion of the turret has an opposite effect - an adverse pressure gradient forms which leads to flow separation and the formulation of a highly-turbulent wake. The turbulent structures created by the flow over the turret create a fluctuating density field that gives rise to index-of-refraction variations in the air. Near the base of the cylinder, a necklace vortex forms and propagates downstream, and in the wake of the turret, and two "horn" vortices form. These flow features are dependent on the Reynolds number until a minimum Reynolds number of approximately 500,000 is reached [1]. Additionally, for incoming Mach numbers larger than 0.55, a shock forms over the top of the turret as the flow becomes locally supersonic [1, 9].

One potential way of improving the aero-optical environment associated with the turret projection platform is utilizing various flow control methods. Flow control schemes seek to modify the turbulent segments of the flow field that are responsible for the aberration of the laser beam. This is accomplished through a variety of methods. For a two-dimensional turret with a flat window, a row of small vertical pins placed upstream to the aperture was shown to improve the aero-optical performance of the turret. These small pins were sufficient to create a secondary shear layer that reduced the strength of the main shear layer over the aperture, with the net effect of reducing beam aberration [6, 10]. A horizontal partition plate mounted in front of the turret has been shown to create an additional necklace vortex around the turret, which, through a non-linear interaction with the turbulent wake downstream of the turret resulted in moving the separation point further aft, reducing the wake size and, consequently, aero-optical distortions at large looking-back angles [11]. Fluidic actuators have also been studied in regards to improving aero-

[1] Graduate Student, Department of Aerospace and Mechanical Engineering, Hessert Laboratory for Aerospace Research, Notre Dame, IN 46556, AIAA Student Member.
[2] Research Associate Professor, Department of Aerospace and Mechanical Engineering, Hessert Laboratory for Aerospace Research, Notre Dame, IN 46556, AIAA Associate Fellow.
[3] Professor, Department of Aerospace and Mechanical Engineering, Cushing Hall of Engineering, Notre Dame, IN 46556, AIAA Fellow

optical performance of turrets. They have also been shown to delay separation on a hemisphere-on-cylinder turret, especially in combining with passive flow control using the partition plate [11]. Suction has been extensively studied as a flow control method for turrets through CFD [8]. Additionally, in recent years, closed loop flow control has been performed using a pitching turret to reduce turbulence intensity over the aperture [12].

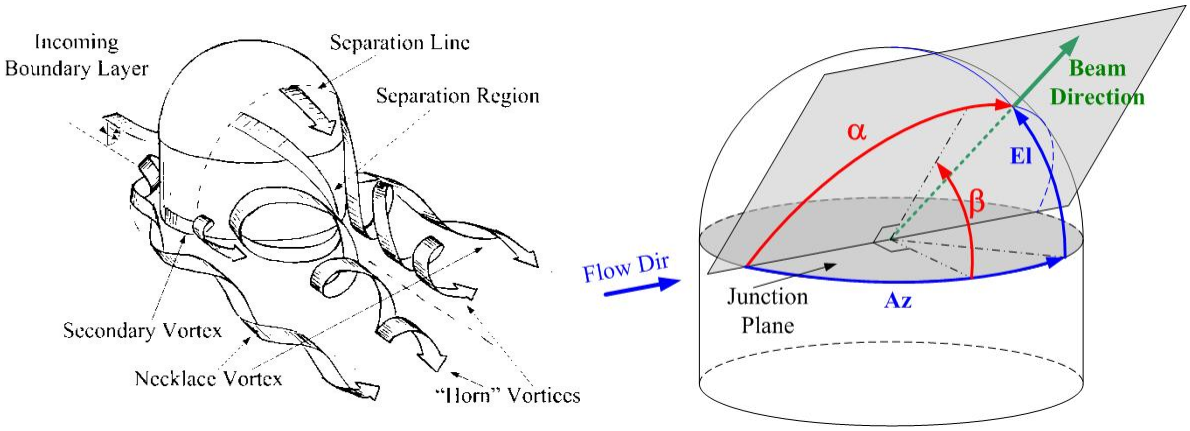


Figure 1. Left: The dominant flow structures around a hemisphere-on-cylinder turret, from [1]. Right: the turret viewing angle definitions.

Vortex generators (VGs) provide another potential method of improving the aero-optical environment around turrets. They are passive flow control devices, not requiring any control scheme to work. Additionally, they are placed off of the turret body itself, meaning that implementation of flow control via VGs doesn't require any modifications to an existing turret assembly. The goal is to introduce streamwise vortical structures into the wake of the turret and to achieve an effect of delaying the separation and/or modifying the wake, similar to what was accomplished with the partition plate in [11]. In this paper, a parametric RANS-only CFD study was performed to investigate the effect of VG position and its angle on the entire flow field around the hemisphere-on-cylinder turret. Guided by CFD results, tunnel experiments were carried out in a wind tunnel to investigate the aero-optical effects of the VG placement. These experimental results had proven the trends seen in CFD simulations. Guided by these parametric studies, a final VG configuration was tested in-flight using the AAOL.

### A. Tunnel set-up

The wind tunnel testing was performed at the University of Notre Dame in the White Field Mach 0.6 wind tunnel. The turret was mounted on the bottom wall of the wind tunnel, see Figure 2, top plots for the schematic and picture. The vortex generators were mounted on the tunnel wall symmetrically on both sides of the turret at different locations and angles of attack. VGs were 8 inches in length, $1/8^{th}$ of an inch thick and 4 and $7/8^{th}$ inches tall. Two different tunnel tests were performed. For the first test, a total of 10 different VG locations and angle-of-attack configurations were tested, shown in Figure 2, bottom plots. The VG angle of attack was set to either 20° or 30°. This tunnel testing was done at M = 0.25 and M = 0.3. The optical setup is shown in Figure 3. A slowly-diverging laser beam from a laser at 50 meters away from the turret, to match the distance between planes in flight, was steered at a prescribed elevation/azimuthal angle onto the turret aperture using mirrors. The turret has a telescope consisted of series of mirrors and lenses, so the incoming beam was contracted from 4 inches to 20-mm beam and re-imaged to the FSM system, see Figure 3. The closed-loop FSM system eliminates the majority of jitter imposed on the beam, and the resulting stabilized outgoing beam is then re-imaged on the Shack-Hartmann wavefront sensor with 32x32 sub-aperture resolution and a temporal resolution of 25 kHz. Additionally, residual jitter measurements are taken using a Position Sensing Device (PSD) at 100 kHz simultaneously with the wavefronts. The tunnel data for the first tunnel test were acquired at a fixed azimuth angle of 139.3° and elevation angle of 28.7°.

The second tunnel test was run in the same tunnel at the same Mach numbers as the first test. The VGs were mounted at an angle of 29 degrees with respect to the flow direction, and the front was 12 mm upstream and 180 mm cross-stream of the turret midpoint, indicated by a thick line in Figure 3, bottom left. This VG location was shown to be an optimal VG placement from both the numerical simulations and the first tunnel tests; the same VG location was used in flight. Data were acquired over a range of back-looking viewing angles to investigate angles that were un-obtainable in flight, due to line-of-sight limitations imposed by the two aircraft. This includes holding the azimuthal angle at 156° and varying elevation angles from 10° up to 50°, as the elevation angles below 30°, in

particular, cannot be achieved in flight. The same Shack-Hartmann 2D wavefront sensor and the optical setup were used, as for the first test.

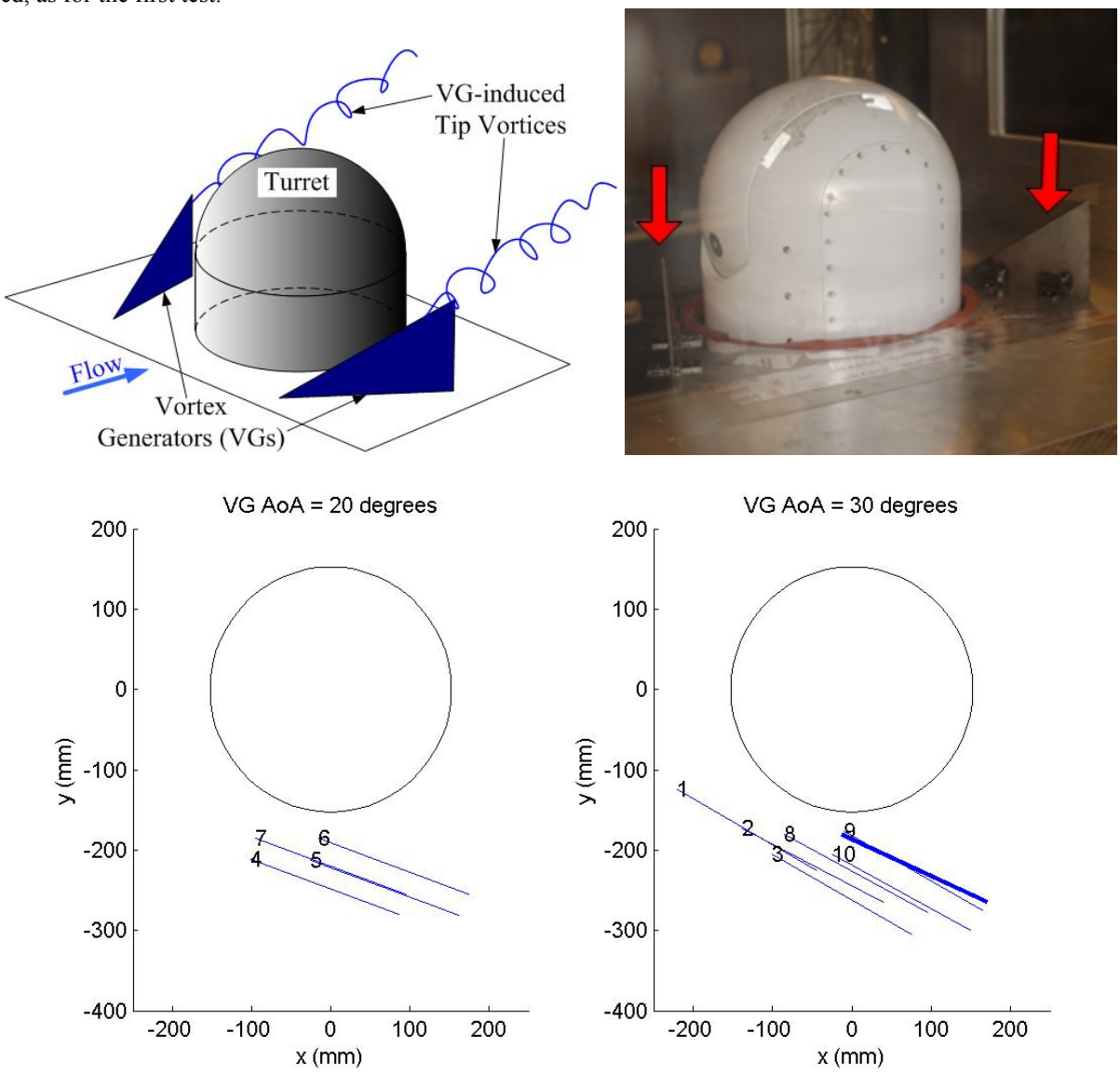


Figure 2: VG locations for tunnel test. Top left: schematic of VG locations. Top right: The turret mounted in the tunnel with the VGs. The arrows indicate the VGs. Bottom left: VG locations at 20° angle of attack for the first tunnel test. Bottom right: VG locations at 30° angle of attack for the first tunnel test. Only one VG is shown for clarity, with another one placed symmetrically on the opposite side of the turret. The thick line indicates the VG position used for in-flight and second tunnel tests.

**B. Flight Set-Up**

The AAOL program utilizes two aircraft flying in closed formation to obtain in-flight aero-optical measurements, for more information of the AAOL program [13], as only essential details will be described here. The first of these aircrafts, designated the laser aircraft, projects the laser onto a turret mounted in the second aircraft, the laboratory aircraft. The aircraft maintain a separation of approximately 50 meters in flight. The laser is projected out of one of the aircraft window of the laser aircraft via a mirror on a gimbal and tracks the turret aircraft using reflections of the laser off the turret itself. The laser is diverging between the two aircraft; it begins as a small aperture beam and overfills the turret aperture by a factor of 2 at the 50 meter distance. This considerably lessens the tracking requirements of the source beam compared to those of the turret itself. On the second aircraft, designated as the laboratory aircraft, the turret is mounted through a modified escape hatch. The turret's azimuthal and elevation

angles are controlled by brushless motors. It tracks the laser aircraft with two different Position Sensing Devices (PSDs). The turret is capable of being fitted with both flat and conformal windows. To prevent condensation on the optical components, which would result from the large temperature differentials between ambient air at differing altitudes, the turret is continually flushed with dry air.

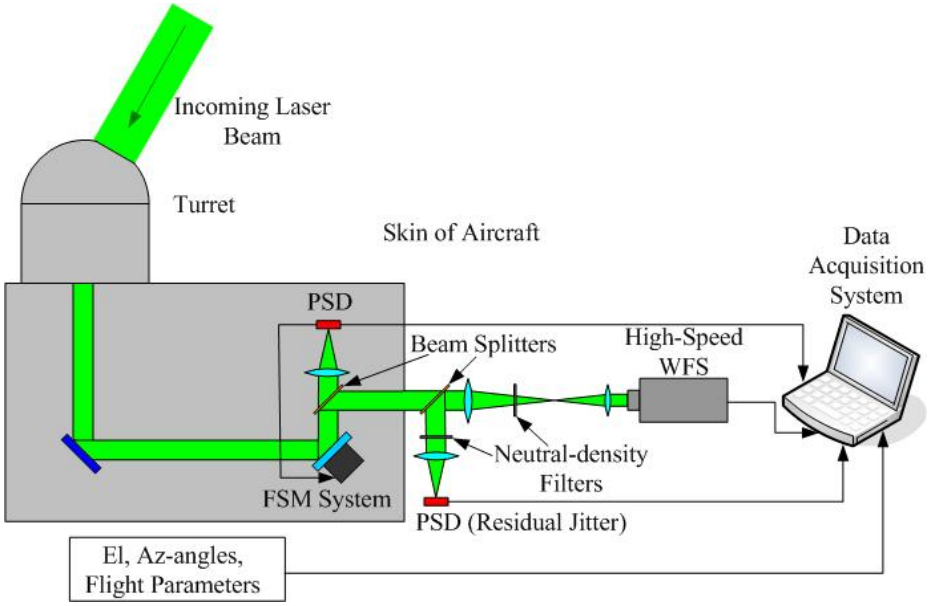


Figure 3: Right: The schematic of the optical setup for the flight and tunnel tests.

Figure 4: The vortex generators mounted on the AAOL. The flow goes from right to left.

The vortex generators mounted on the plane can be seen in Figure 4. The VGs are in the same location in flight relative to the turret as for the second tunnel test, indicated by a thick line in Figure 3, bottom left. The VGs were bolted directly to the aircraft escape hatch using 6 L-brackets. In all flight tests the VGs were mounted normal to the surface, and as a result, the curved wall of the aircraft provides a slight geometric difference from the CFD and tunnel tests, which featured the turret mounted to a flat plate.

The experimental setup inside the laboratory aircraft is shown in Figure 5. The optical setup is identical to that used in the tunnel tests, which is shown in Figure 3. Flight conditions and the current turret azimuth and elevation angles are also acquired simultaneously with optical measurements. The two aircraft are equipped with a differential GPS system which allows for acquisition of the displacement between the aircraft as well. The jitter data and GPS data will not be presented here, but analysis of the jitter data for other flight tests on the AAOL can be found in [13].

Flight data was acquired at Mach numbers of 0.5 and 0.65. For M = 0.5, the aircraft flew at an altitude of 15,000 feet, but for M = 0.65, a higher altitude of 28,000-34,000 feet was used. In this paper, only the results of M=0.5 will be presented and discussed. Data were acquired in one of two modes: a fixed-angle or a slewing maneuver. Fixed-angle data were obtained with the aircraft maintaining a fixed position with one another, and for these cases, 15,000 wavefront frames were acquired at the full 25 kHz. Slewing maneuvers involved the laser aircraft slowly moving with respect to the laboratory aircraft. For this case, the Shack-Hartmann sensor acquired 21,000 frames at a rate of 3 kHz. The fixed angle data allows for fully time-resolved wavefront measurements, while the slewing maneuvers allow for the computation of statistical quantities over a large range of viewing angles. For the slewing maneuvers, the statistical quantities are computed over 1,500 frame subsets; this corresponds to averaging over half-second segments. It has been previously shown that this is sufficient for statistical convergence [2]. For more details of wavefront reduction techniques used, see [3].

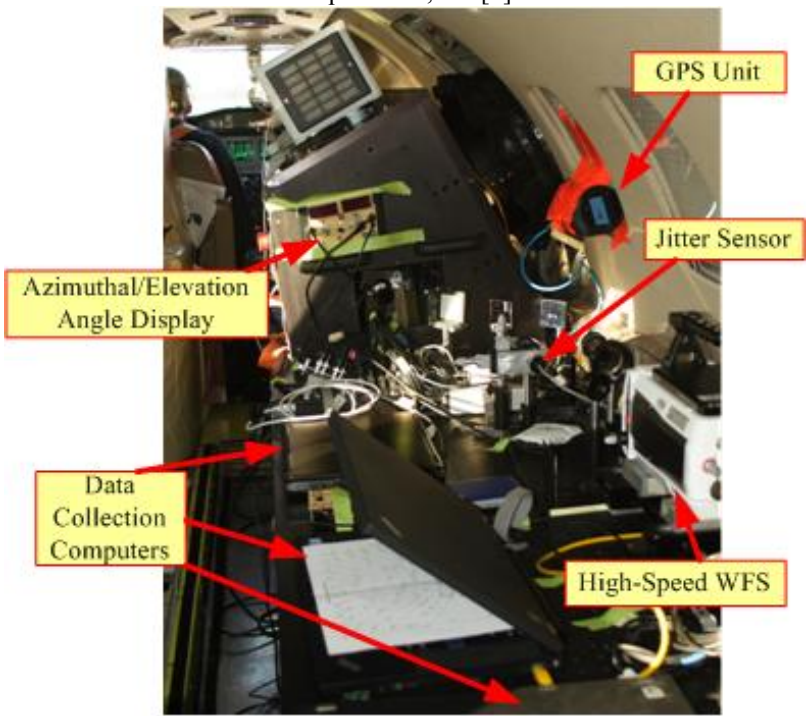


Figure 5: The interior of the turret aircraft.

The processing of wavefront data gives two dimensional spatial wavefronts as a function of time, $W = W(x, y, t)$. The residual tilt was removed from each wavefront by fitting a least-squares plane. The time-averaged component was also removed from each wavefront to eliminate the steady lensing. The mean $OPD_{RMS}$, which characterizes the average amount of wavefront spatial variation over the aperture of the wavefront, is computed by time-averaging the spatial RMS of frame, $\overline{OPD_{RMS}} = \overline{\sqrt{\langle OPD(x,y,t)^2 \rangle_{x,y}}}$, where the angular brackets indicate spatial averaging. For slewing maneuvers, this averaging occurs over 0.5-second subsets, to ensure that the flow conditions imprinted on the laser are not varying over subset as the viewing angle is continuously changing during the slewing maneuver. As the aircraft separation is not necessarily constant over a slew maneuver, a slow defocus can be imparted on the beam that is independent of any aero-optical effects. To eliminate this effect, steady lensing is removed for each of the 0.5-second subsets, as the aircraft separation is approximately constant at this timescale.

To characterize the optical distortions caused be the turret, at each fixed point and 1,500 frame slewing maneuver subset, the time-averaged level of aero-optical distortion, $OPD_{RMS}$, was computed. This was then normalized for comparison across different flight conditions using the flight conditions. This scaling has been previously shown in [1,2] and is given by

$$OPD_{Norm} = \frac{OPD_{RMS}}{\left(\frac{\rho_0}{\rho_{SL}}\right) M^2 D}.$$

In this relation, the free stream density is $\rho$, while the density at sea level is $\rho_{SL}$. The diameter of the turret is given by $D$, and $M$ is the free stream Mach number. Note that the units of normalized $OPD_{RMS}$ reported in this paper

are μm/m. This scaling assumes that the flow topology doesn't change as Mach number changes. For instance, it breaks down as flow transitions to the transonic regime when a shock forms on the turret.

The normalized spatial distribution of $OPD_{RMS}$ was also computed for the tunnel cases. This is done by computing the temporal variation of the OPD at each subaperture, $OPD_{RMS}(x,y) = \sqrt{\langle OPD(x,y,t)^2 \rangle_t}$. This is a convenient statistics to quantify the local contribution of various parts of the aperture to the mean $OPD_{RMS}$, as well as it can provide insight into the flow physics at work [2,3].

The azimuthal and elevation angles are also redefined to a more convenient system from a flow-physics perspective, as the viewing angle, $\alpha$, and the modified elevation angle, $\beta$, coordinate system, see Figure 1, right,

$$\alpha = \cos^{-1}(\cos(Az)\cos(El)) \text{ and}$$
$$\beta = \tan^{-1}(\tan(El)/\sin(Az)).$$

The viewing angle,, α. describes at what angle downstream the turret is looking and the modified elevation angle, β, determines how far away from the aircraft fuselage the turret window is looking.

## 2. Results

### A. CFD and First Tunnel Study Results

Steady-state CFD parametric studies were performed using AVUS, a RANS solver using the Wilcox k-ω wall model. The grid had 1.4 million cells, and each case ran for 50,000 time steps, with a $\Delta t = 3 \times 10^{-5}$ second. The flow was simulated at a freestream Mach number of 0.4. The simulations were stopped when the steady state was reached and the boundary layer at the turret was sufficiently large for the necklace vortex to exist. The CFD modeled the VGs in a tunnel test setting specifically, the open-air performance, as experienced in flight was not directly simulated.

Figure 6 shows the results of the VG parametric CFD study. A variety of VG position and angle combinations were investigated, numbering 13 simulation cases in total. Going from the baseline flow, Figure 5, top plots, to the VGs at a 20 degree angle with a maximum distance from the turret of 1 diameter, the flow does not change substantially; see Figure 5, middle plots. The only difference is that the necklace vortex being pulled away from the wake slightly far aft of the turret. Aero-optically, this configuration was not expected to impact the turret performance much, as the flow topology in the near field of the turret is almost entirely unchanged. To achieve a substantial change in the flow topology, the VGs were moved much closer to the turret. Figure 5, bottom plots, shows the CFD for the configuration that was actually flown in flight. By placing the VGs closer to the turret, the necklace vortex was actually pushed significantly outwards compared to the baseline case. The increased angle of attack further helped the displacement of the necklace vortex.

The VG numerical study provided guidance for the first tunnel study in which aero-optical data were acquired at M=0.35 for a fixed angle of α = 132°, β = 40°. Ten different VG positions were tested in the tunnel experiments, see Figure 2, bottom plots. Comparing $OPD_{RMS}$ between the baseline and the tested VG cases, similar trends were observed. The mean OPDrms value for the baseline cases was approximately 1.519 μm/m. With VGs at Locations 9 and 10, respectively, shown in Figure 2, bottom, this value was reduced to 1.407 μm/m and 1.444 μm/m, respectively. From these preliminary results, the decision was made to do the flight testing using Location 9 configuration.

As seen from CFD results, the VGs modified an already complex and three-dimensional flow field. Our hypothesis for the change to the flow field and the observed optical effect from VGs in this configuration is as follows. Near the VGs, several distinct changes occur in the flow: the necklace vortex is pushed away from the turret, the VGs introduce an additional tip vortex, schematically shown in Figure2, top left, and the local flow expansion effect between the turret and the VGs creates a pressure drop, possibly accelerating the flow around the cylindrical portion of the turret. These effects impact the structure of the wake; the horn vortices are pulled outward, away from the 180° azimuth direction. Aero-optical performance at side-looking angles should be relatively unchanged as the VGs are downstream of the turret center. The downwash on the wake from the necklace vortex alone will decrease, as it is moved away from the wake center, but the additional tip vortices from the vortex generators will mitigate this. At small elevation angles, for Az > 120-130°, the aperture will be looking directly through a portion of the tip-vortex, significantly aberrating the laser beam. Looking through the wake alone, the combined downwash from the tip-vortex and necklace vortex may reduce the vertical extent of the wake, providing improvement at very back-looking angles (α > 120°). As the necklace vortex has been forced away from the turret and the tip-vortex likely isn't fully developed, the downwash near the turret itself will likely not have changed enough to impact the location of the separation line on the turret. If any change in separation line location occurs, it

will be at large azimuth (Az > 130°) and low elevation (El < 30°) where the turret surface is close to the vortex generators and pressure field is changed the most. In this region, the effect of the downwash will be maximized and the overall pressure gradient may become more favorable by the pressure decrease behind the VGs. Finally, a significantly-smaller values in optical aberrations has been observed at back-looking angles at a very large ($\beta > 80°$) modified elevation angle [2,3]. This is the result of looking between the two horn vortices. With the horn vortices pulled outward from the wake center by the VGs, this region of reduced aberration may increase in size and be observed at smaller $\beta$ angles.

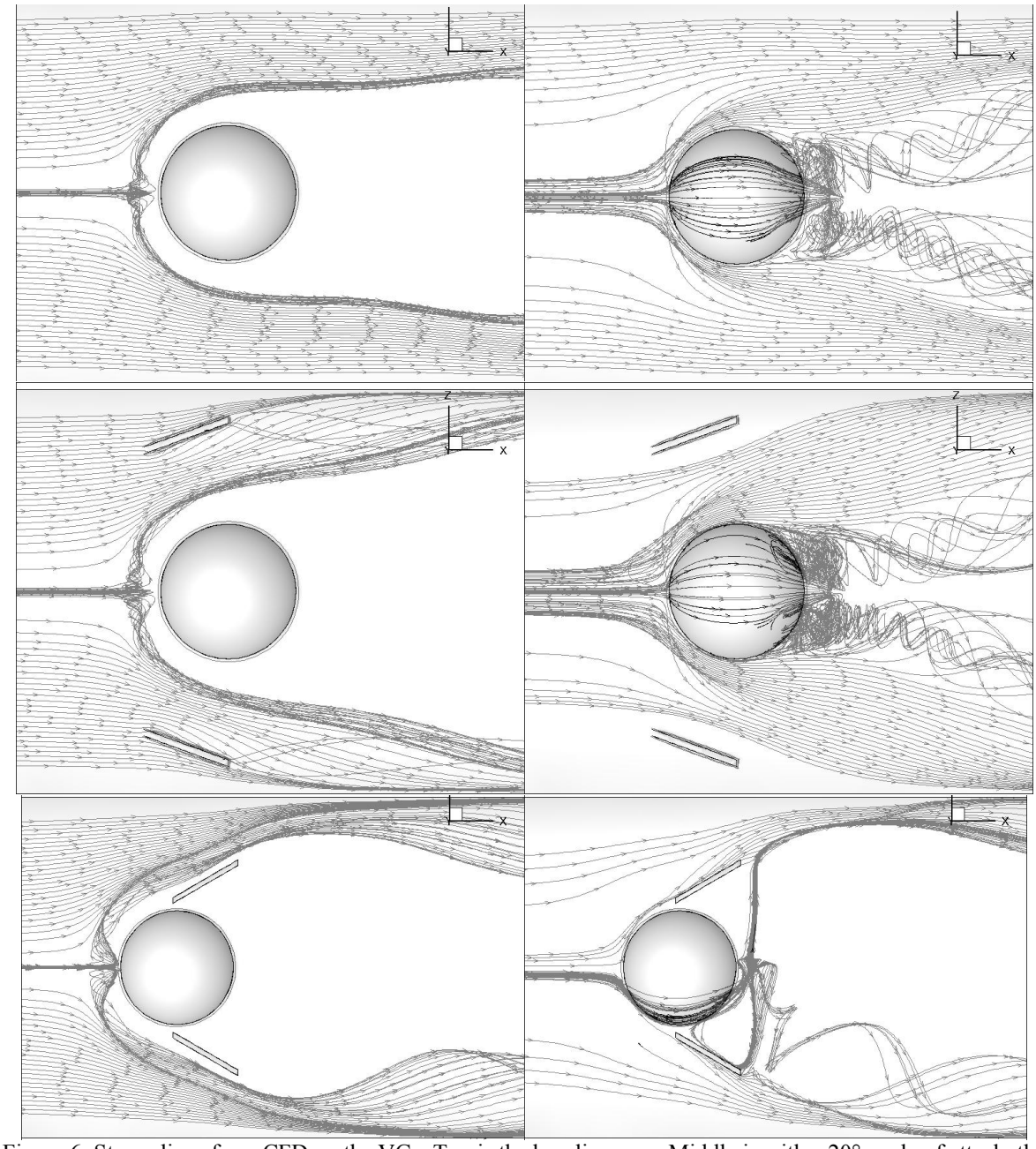

Figure 6: Streamlines from CFD on the VGs. Top is the baseline case. Middle is with a 20° angle of attack, the trailing edge of the VGs 1 diameter from the turret and in line with the centerplane. Bottom is with the leading edge of the VGs approximately an inch from the turret and a 30° angle of attack. Left are streamlines near the base of the turret and right are streamlines further off of the plate the turret is mounted on.

**B. Flight and Second Tunnel Study Results**

Full discussion of baseline aero-optical properties of turrets can be found in [2,3], so here we highlight only essential features, relevant to understanding the VG impact. Figure 7 shows normalized $OPD_{RMS}$ values obtained in-flight and in the tunnel divided into specific β-ranges. The tunnel data for 120° < α < 130° show a modest improvement by the VG, compared to the baseline case. Unfortunately, no reliable experimental data are available from in-flight, VG experiments. In this viewing angle range, the location of the separation line and the dynamics of the recirculating region were mostly unaffected by the vortex generators, consistent with the proposed hypothesis. At α > 130°, there is a reduction in $OPD_{RMS}$ with the vortex generators. In this α-range, our hypothesis states the VGs reduced the vertical extent of the wake, consequently reducing $OPD_{RMS}$ as the laser beam integrates through the smaller wake region. For 50° < β < 70°, Figure 7 right, at α < 110° there is a moderate increase in $OPD_{RMS}$ values of approximately a factor of 2; the reason for this increase is not quite clear at this moment. For α > 110°, $OPD_{RMS}$ values for VG case follow those of the baseline, until α > 120°. Above α =125°, there is a marked decrease in $OPD_{RMS}$ values. The improvement can again be explained by a reduction in the vertical extent of the turret wake, but the increase at at α < 110° is not directly explained by our hypothesis. From these experimental results, the tested VG configuration gives a marked improvement in a very specific viewing angle range, although no flight data are available for viewing angles α > 130° to see whether the mitigating trend continues. Additionally, VGs can actually worsen the optical aberrations in viewing angles below 110 degrees. This issue can be avoided by, for instance, retracting VGs for some angles and deploying them for other angles.

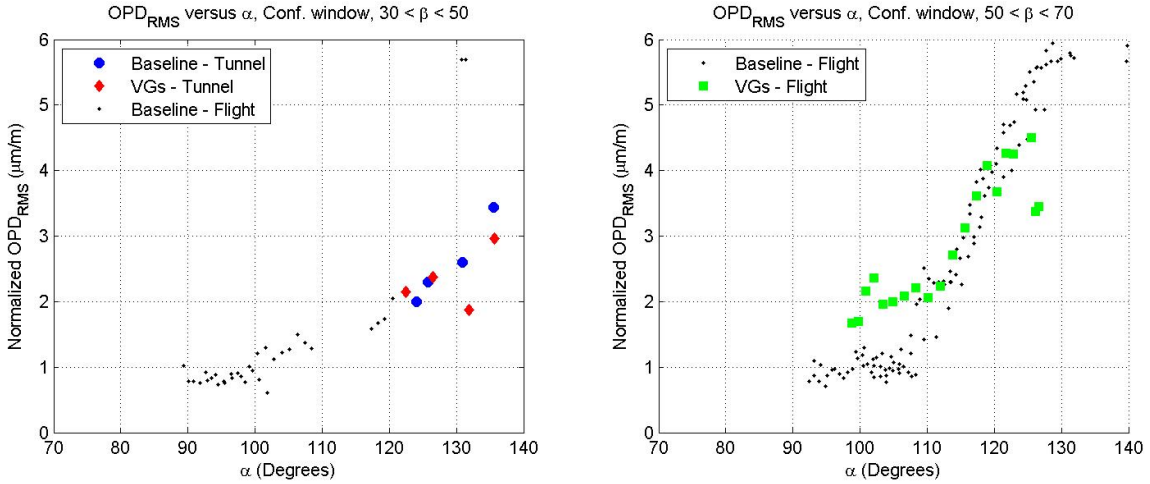


Figure 7: $OPD_{RMS}$ versus viewing angle, α, for VG and baseline cases with a conformal window. Left plot shows 30° < β < 50° while right plot shows 50° < β < 70°.

Figure 8 gives the spatial distributions of $OPD_{RMS}$ for the tunnel data. At Az = 132°-136°, the VGs have a little effect on the spatial distribution of $OPD_{RMS}$. Looking further downstream, at Az = 142°, there is a substantial reduction in $OPD_{RMS}$ values for the VG case, particularly on the downstream portion of the aperture. In the baseline case, there is a steady progression to larger $OPD_{RMS}$ values moving from the upstream to downstream portion of the aperture. This is the result of looking through a spatially-growing vortical structures formed after the flow separates off the turret. At this angle, the VGs significantly modified the dynamics of the vortical structures in the separated flow region. This is most probably due to the aperture been close enough to the VGs that the downwash and pressure drop behind the VGs delayed the separation. Looking further downstream through the wake itself, at Az = 146°, the VGs also showed a reduction in local $OPD_{RMS}$. The aberrations observed on the upstream portion of the aperture are relatively unchanged between the baseline and VG cases, while the downstream portion shows smaller levels of temporal $OPD_{RMS}$ for the VG case. This is consistent with the hypothesis that the VGs reduced the overall extent of the wake near the aperture at these viewing angles.

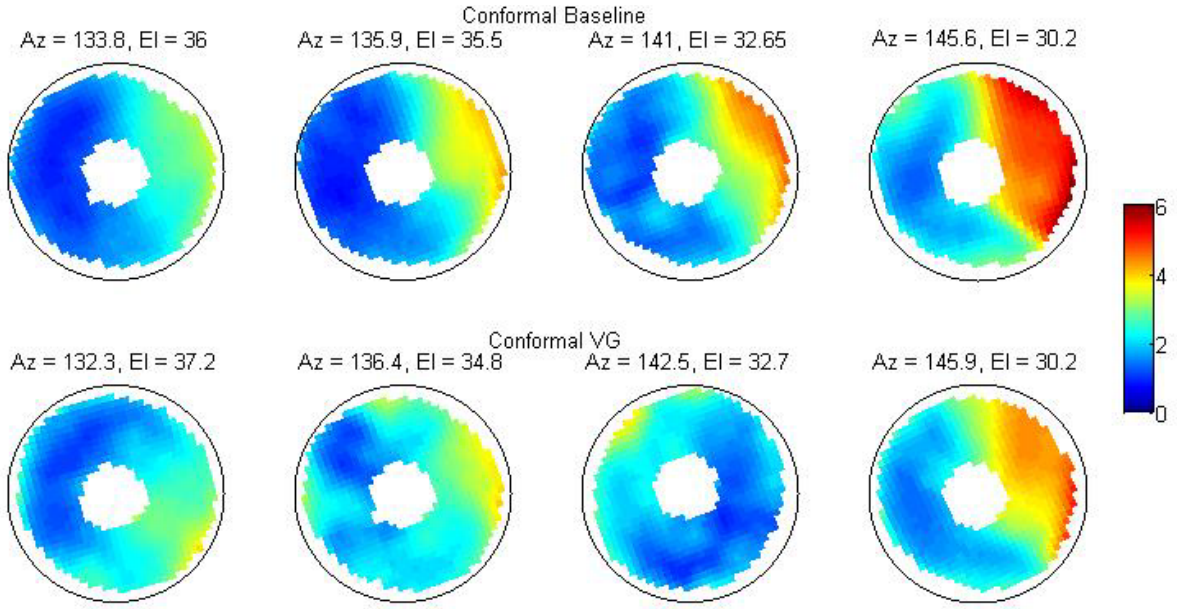


Figure 8: Spatial distribution of normalized $OPD_{RMS}$ from tunnel data for baseline and VG cases at various angles (in degrees) for the conformal window. The black circles indicate the aperture of the turret. The distributions are in the frame of reference of the aperture, with the vertical direction pointing towards the turret apex. The flow direction is approximately left-to-right.

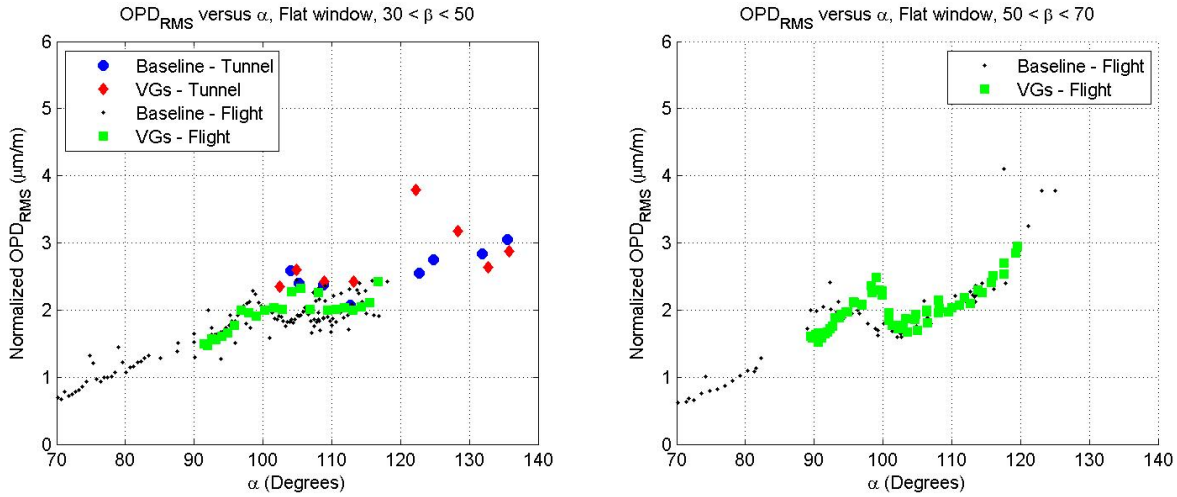


Figure 9: $OPD_{RMS}$ versus viewing angle, α, for VG and baseline cases with a flat window. Left plot shows 30° < β < 50° while right plot shows 50° < β < 70°.

Figure 9 shows $OPD_{RMS}$ values for the flat window, with and without the VGs. As it was discussed in [2, 6] there is a local peak in $OPD_{RMS}$ for flat-window turrets for the viewing angle between 90 and 100 degrees that results from the combination of the formation of the local separation bubble over the flat-window surface and the global tip/tilt removal from wavefronts at this viewing angle range; the location of this local peak was shown to depend on the modified elevation angle, β. The α-angle at which separation occurs over the flat window increases as β decreases. This is shown by the location of the local peak in the $OPD_{RMS}$ shifting to larger values of α as β decreases. With the VGs present, the local peak is somewhat suppressed for 30° < β < 50°. This indicates that the VGs were modifying the flow over the flat window at these angles, as it is possible that the downwash effect of vortices introduced by the VGs was mitigating the adverse pressure gradient introduced by the flat window itself. It is possible that the increased downwash was sufficient to impact this local separation while leaving the wake separation line on the turret unchanged. There is a modest local increase in in-flight $OPD_{RMS}$ for the flat window in

the 103° < α < 107° range, which might be due to the experimental error, casing the data scatter, as the tunnel data showed that VGs had no discernible effect for these angles of α < 120°. For the flat window, there is a marked increase in $OPD_{RMS}$ for the VG case at 120° < α < 130°. The exact reason for this effect is not quite clear, as there were no VG data collected in-flight for this angle range. One main difference between the flight and the tunnel experiments was that the tunnel data were collected at a lower M = 0.25, while the in-flight data were collected for M=0.5; the second difference was the tunnel blockage. In [1] it was shown that the flow around the turret have residual transitional effects for $Re_D$ <500,000, which corresponds to M=0.4 for the tested turret. Therefore, one possible explanation might be that at lower speeds the additional pressure gradients created by VGs in the wake negatively interacted with the adverse pressure gradient over the flat window, creating stronger vortical structures over the window. Similar to the conformal window, there is a reduction in $OPD_{RMS}$ for the VG case at α > 130°, though the magnitude of the effect is less. This indicates that the flat window geometry might limit the mitigation factor of the VGs in the wake.

For 50° < β < 70°, the location of the local peak in $OPD_{RMS}$ is pushed to smaller values of α = 98-100°. As mentioned before, the vortices generated by the VGs should also induce a stronger downwash near the window; this has the effect of accelerating the flow over the turret. At the larger β angle, the aperture is further from the tip-vortex and necklace vortex, so the induced downwash effect should be reduced. This is consistent with the fact that the peak isn't suppressed, as observed for 30° < β < 50°, but only delayed. After the peak, the VGs do not increase or decrease the observed $OPD_{RMS}$ with the flat window. This is the same as observed for the conformal window at α < 125° and predicted by the proposed model, where the separation line is unaffected for larger β.

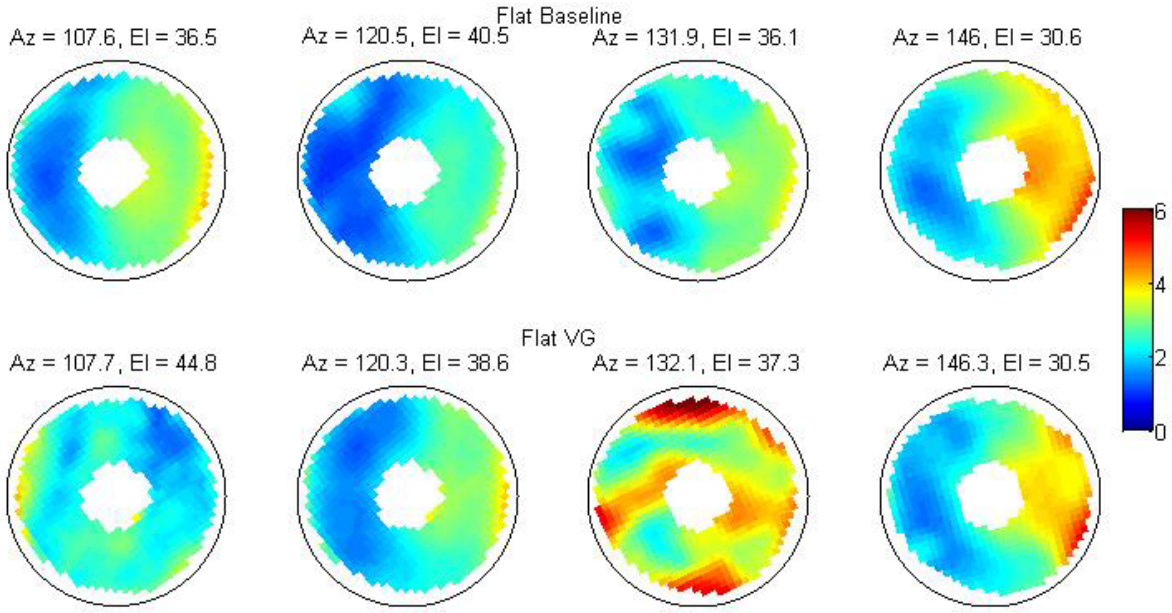


Figure 10: Spatial distribution of normalized $OPD_{RMS}$ from tunnel data for baseline and VG cases at various angles (in degrees) for the flat window. The black circles indicate the aperture of the turret. The distributions are in the frame of reference of the aperture, with the vertical direction pointing towards the turret apex. The flow direction is approximately left-to-right.

The spatial distributions of $OPD_{RMS}$ for the flat window are given in Figure 10. The VGs were modifying the gradual increase in $OPD_{RMS}$ along the flow direction observed in the baseline over the flat window at Az = 107°, but the average $OPD_{RMS}$ over the aperture was not changed significantly. At Az = 120°, the turret began to look through the separated wake, and the VGs again were not changing the magnitude of the distortions. For Az = 132°, the VGs introduce substantial aberrations into the beam. This is specific to the flat window; as shown in Figure 8, the VGs don't affect the optical distortions observed over the conformal window at this angle. As mentioned before, it is likely that there is some complex interaction between the adverse pressure gradient observed over the flat window and the expansion of the wake caused by the VGs. At Az = 146°, the turret is looking into the wake, and the VGs have a very slight reduction effect on the distortions observed in the downstream portion of the aperture.

The time-average autocorrelation maps of the wavefronts for the flat window case at these four angles are shown in Figure 11. For Az = 107°, the baseline shows stronger negative correlation values in the streamwise

direction than for the VG-case. This indicates that the VGs were disrupting the development of the turbulent vortical structures convecting across the aperture at this angle. Additionally, the elongation of the center peak in the cross-stream direction indicates the size of those structures in the vertical direction. For the VGs, the center peak is less elongated in the cross-stream direction. This is further indication that VGs were modifying the structures convecting over the aperture. At Az = 120°, the autocorrelations are relatively unchanged and it is consistent with the spatial distribution of $OPD_{RMS}$ results at this angle, seen in Figure 10. The autocorrelation at Az = 132° is substantially changed between the flat and VG cases. Instead of the typical negative correlation upstream and downstream of the aperture center, observed in the baseline, there is substantial negative correlation in the cross stream direction. This indicates that the VGs were completely changing the flow over the flat aperture at this angle. As mentioned, this is possibly the result of a complex interaction between the expansion of the wake by the VGs and the shape of the flat window. For Az = 146°, there is again minimal change in auto-correlation maps between the baseline and VG cases. While the VGs slightly reduced $OPD_{RMS}$ at this angle, they did not change the flow structure significantly. This result is expected if the downwash of the VGs is reducing the vertical extent of the wake; the amount of turbulence the beam propagates through would be reduced, but its structure would be unchanged.

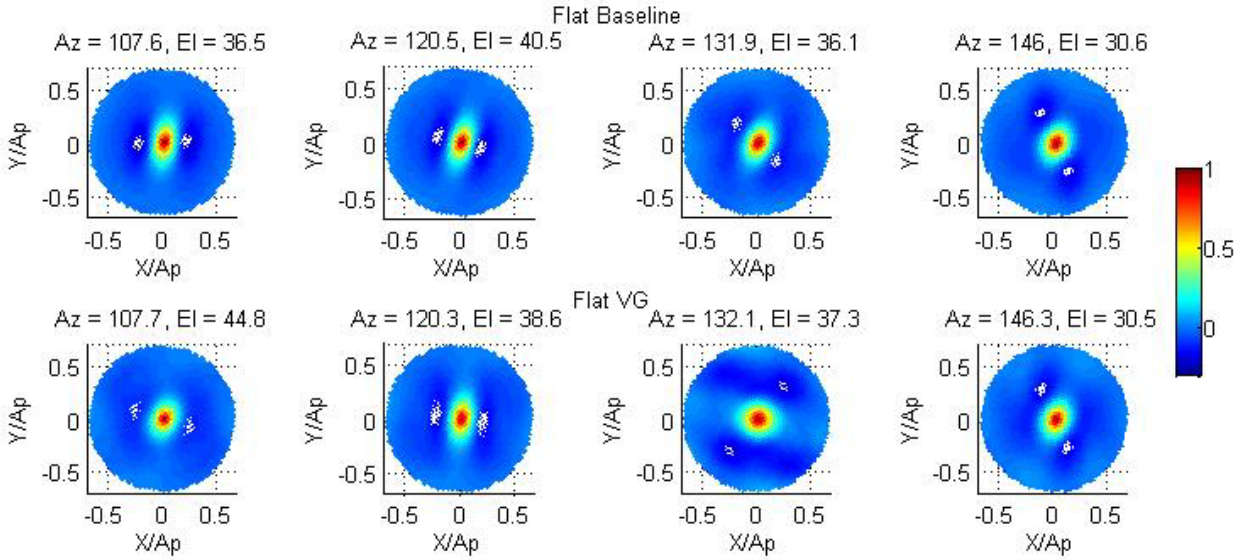


Figure 11: Normalized autocorrelation maps for the baseline and VG cases with the flat window. The maps are in the aperture frame of reference, with flow direction being approximately left-to-right.

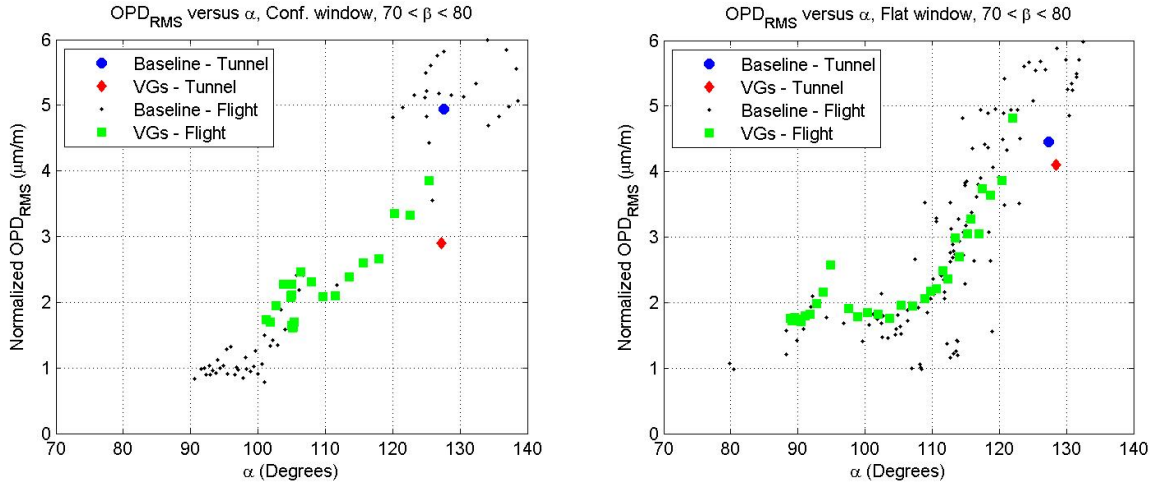


Figure 12: $OPD_{RMS}$ for 70° < β < 80°. Left plot is for the conformal window, and right plot is for the flat window.

Given the previously-shown positive mitigation effect that the VGs had when the window was looking through the wake at 50° < β < 70° and α > 125° with the conformal window, it is expected that this would continue for 70° < β < 80°. The $OPD_{RMS}$ values for this β range are given above in Figure 12. In the case for the conformal window, see Figure 12, left, there is a decrease in $OPD_{RMS}$ for α > 120°. This is especially shown with the tunnel data, where there is a reduction of almost 40% in $OPD_{RMS}$. These would be consistent with the model that the VGs are reducing the vertical size of the wake. In particular for the tunnel case, a large reduction may be the expansion of the aero-optically quiet zone between the two necklace vortices that was predicted by the model. It should be re-iterated, though, that the lower Mach number and blockage in the tunnel might also be amplifying this effect, and it may not be achievable for higher Mach numbers. For the flat window, $OPD_{RMS}$ for VG case essentially follows the same pattern as for the baseline case. It is expected that the VGs have limited effect on the separation line at large β angles. The tunnel data also shows little difference between the VG and baseline cases at α > 125°, the same location that the large drop was observed for the conformal window, further indicating that the presence of flat window may be interacting with the modified wake, reducing the mitigating effects from VGs.

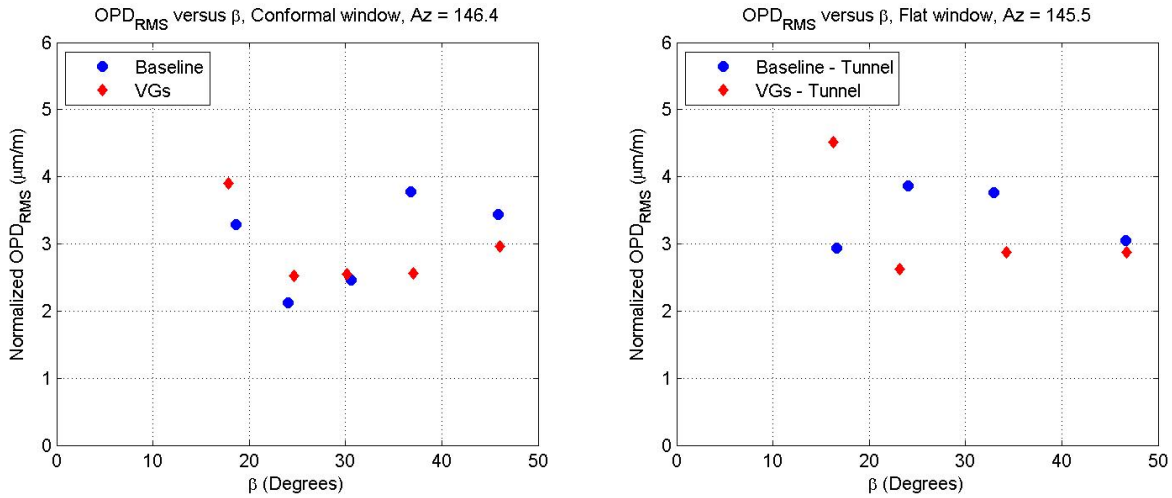


Figure 13: $OPD_{RMS}$ obtained in the tunnel at Az = 145-146 degrees (144 > α > 135, depending on elevation angle). Left plot shows data for the conformal window, and right plot shows data for the flat window.

A further investigation into the modified-elevation angle dependence on the VG effects was performed in the tunnel during the second test. The normalized $OPD_{RMS}$ values are given in Figure 13 for a fixed azimuthal angle of approximately 145 degrees. For this azimuth angle, a common trend is seen for both windows. For VG cases, results exhibit larger $OPD_{RMS}$ values at smaller β, and smaller values than the baseline at larger β. This is consistent with what was observed in the flight data; at small β, the laser is projected through the additional wake from the VGs, causing an increase in $OPD_{RMS}$. As β increases, the laser moves away of this wake, and the downwash effect of the VGs reduces the size of the separated region. The $OPD_{RMS}$ values of the VG and baseline cases approach each other as β approaches 50°. This is likely unrelated to the VG line-of-sight turbulence-reducing effect, as β-angle increases with the azimuthal angle held constant, and α-angle decreases. Thus, for these plots, the larger β angles are moving closer to the separation line, which the VGs are not expected to affect.

Figure 14 gives the spatial distributions of $OPD_{RMS}$ for the conformal window at the same angles as shown in Figure 13, left. At El = 10°, the VG case has significantly more distortions at the bottom of the aperture. At this viewing angle, the laser beam mostly probably was traversing directly through the tip vortices caused by the vortex generators themselves. The baseline case also has distortions at the bottom of the aperture, but with significantly-less magnitude. These distortions are likely caused by the local vortical structures developed over other geometrical features of the turret like "smiles", which is discussed in details in [15]. As elevation angle increases between 15° and 20°, the laser beam was no longer traversing through VG-related wake, and the spatial distributions between the VG and baseline cases are relatively similar. The turret begins looking into the separated wake at El > 22°, with a similar spatial distribution as shown in Figure 8. In this range, the wake is present but introduces smaller aero-optical distortions in the VG case, consistent with prior results and the proposed model.

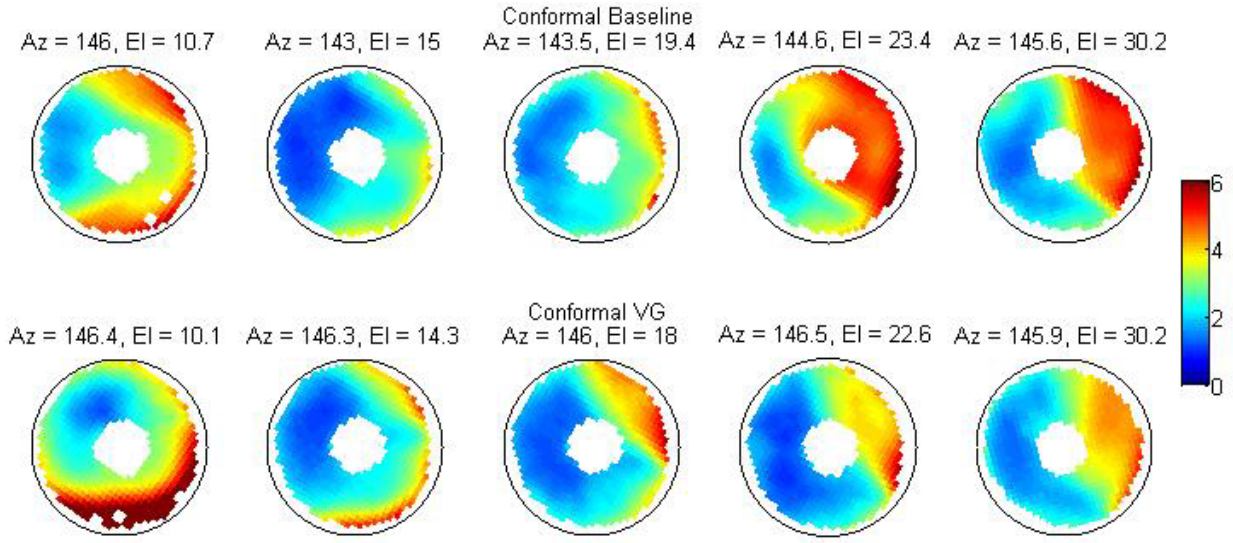


Figure 14: Spatial distribution of normalized $OPD_{RMS}$ from tunnel data for baseline and VG cases with changing elevation angle for the conformal window. The black circles indicate the aperture of the turret. The distributions are in the frame of reference of the aperture, with the vertical direction pointing towards the turret apex. The flow direction is approximately left-to-right.

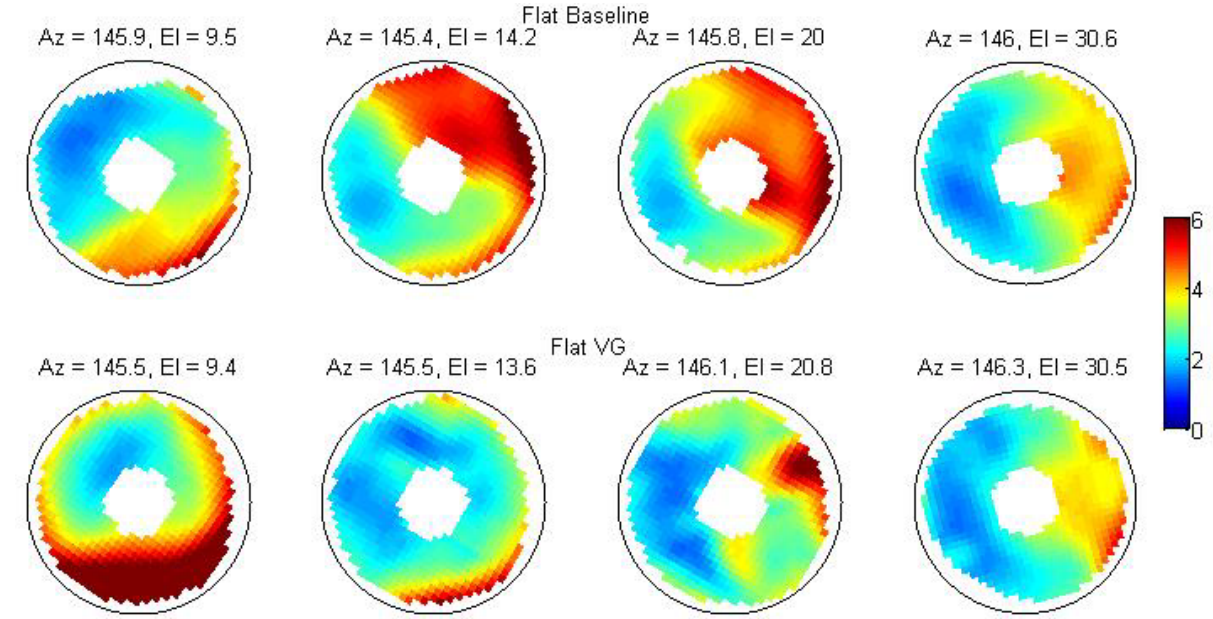


Figure 15: Spatial distribution of normalized $OPD_{RMS}$ from tunnel data for baseline and VG cases with changing elevation angle for the flat window. The black circles indicate the aperture of the turret. The distributions are in the frame of reference of the aperture, with the vertical direction pointing towards the turret apex. The flow direction is approximately left-to-right.

Figure 15 gives the spatial distributions for the flat window as the elevation angle changes. At El < 10°, the same behavior is observed with the flat window as with the conformal one. There is an increase in optical activity in the bottom portion of the window at the low elevation angle, with the VG case having much larger magnitude. For these cases, both the wake of the VGs and the vortical structures formed by the "smile" are separate from the window geometry and thus unaffected by it. The flat window shows the constant streamwise increase in the temporal variation of OPD across it that is indicative of looking through the progressively-wider wake at a smaller elevation angle (14°) than the conformal window. This means that the flat window itself is likely forcing separation to occur earlier and expanding out of the size of the wake in this region; this is also observed at El = 20°. The VGs

disrupt this effect entirely, reducing overall $OPD_{RMS}$ in this region. It is possible that the downwash from the close-proximity tip-vortex and necklace vortex and the low pressure region behind the VGs were mitigating the adverse pressure gradient and forced the flow to stay attached; this is opposite what was observed at larger β angles in Figure 9; smaller Mach number and additional blockage for the tunnel test night be the reason of this reversed behavior. For El = 30°, the beam looks through a thicker portion of the wake and the VGs had a very slight mitigation effect; again, this is very similar to what was observed for the conformal window at this angle. The decrease in the level of aero-optical aberrations observed in the baseline case is due to the aperture moving to a smaller α angle as El increases, thus moving more towards the separation line.

## 3. Conclusions

Numerical simulations, tunnel and flight experiments were carried out to investigate the effects of vortex generators on the aero-optical performance of a hemisphere-on-cylinder turret. A steady-state RANS calculations were performed to investigate the effect of VGs on the global turret flow field for different VG positions. The parametric CFD investigation was used to identify several VG locations to further investigate experimentally in the tunnel. 10 Aero-optical measurements for ten different VG configurations were performed in the first wind tunnel experiment using a Shack-Hartman 2D wavefront sensor with the turret window looking at the fixed angle of Az = 139.3° and El = 28.7°. Guided by first tunnel experiment and the parametric CFD results, an optimal location for the VGs was selected for the flight tests on the AAOL and additional, second testing in the wind tunnel. The final VG orientation was a 30° angle of attack and the front 12 mm upstream and 180 mm cross-stream of the turret midpoint.

In-flight aero-optical measurements were performed using the Airborne Aero-Optics Laboratory. The baseline and VGs were flown at M = 0.5 and 0.65. Wavefronts were acquired with a Shack-Hartmann 2D wavefront sensor. Data was acquired angles using slewing maneuvers to quickly map the aero-optical performance over a large range of viewing angles and fixed points to obtain time-resolved statistics, similar to the procedure, described in [13]. Both flat- and conformal-window geometries were tested. Additionally, a possible model for the predicted aero-optical effects based on the flow around the VGs was provided.

With the conformal window there was an increase in $OPD_{RMS}$ at $50° < \beta < 70°$ for side-looking angles prior to the separation line. However, when the beam was traversed through the separation region, at $\alpha > 125°$ aero-optical levels were decreased for the VG case, as VGs expand the turret wake, reducing the strength of horn vortices and overall turbulent intensity of the wake near the VG. The flat window didn't show the same $OPD_{RMS}$ increase related to the VGs that it was observed with the conformal window as the flow over the flat window is dominated by the separation bubble that forms at side-looking angles. For $30° < \beta < 50°$, the VGs reduced the peak that is associated with this separation bubble; however, for $50° < \beta < 70°$ the peak only moved to a larger α. This is likely due to the downwash effect from VGs, which delayed the separation over the flat window, as it helps to mitigate the adverse pressure gradient that induces the separation. For $70° < \beta < 80°$, the VGs continue to show improvement on the conformal window turret when looking into the separated wake, $\alpha > 120°$. The flat-window turret it showed little improvement.

The conformal window consistently showed improvement when looking far into the wake ($\alpha > 125°$). This is likely the VGs introducing additional downwash on the wake, reducing its vertical extent. The flat window showed less improvement at these far back-looking angles, indicating that the flat geometry is possibly mitigating some of the effect of the VGs when it comes to reducing the vertical size of the wake. Both the conformal and flat windows exhibit regions of increased $OPD_{RMS}$ that were not looking directly through the tip-vortex of the VGs. For the conformal window this was at $\alpha < 120°$ for $50° < \beta < 70°$ and $120° < \alpha < 130°$ for $30° < \beta < 50°$ for the flat window. Neither of these were predicted by the proposed model for the VGs. The flat window also saw a change in the local peak associated with a small separation bubble forming over it. At $30° < \beta < 50°$, it was fully mitigated, while it was only delayed to larger α at $50° < \beta < 70°$. The proximity to the VGs affects the magnitude of the downwash felt over the aperture and likely accounts for the difference between these two.

The VGs were shown to increase optical distortions at the lower El = 10° for both flat and conformal windows. In this range, the beam was traversing directly through the wake downstream of the VGs. As the elevation angle increased, the VGs didn't significantly change the performance of the conformal window until looking into the wake, at El > 23°, where the aforementioned decrease in $OPD_{RMS}$ occurs, likely due to the reduced vertical size of the wake. The geometry flat window introduces separation earlier, at El = 14°, but the VGs break up this separation entirely, greatly improving $OPD_{RMS}$. In this region, the proximity of the aperture to the VGs and and low pressure region behind the VGs prevent this separation. Once again, increasing the elevation angle to 30° and moving into the wake, the VGs have a more limited effect on the aberrations observed using a flat window.

This configuration of VGs has been shown to be very effective in a few angle ranges: $\alpha > 125°$ for the conformal window, with reduced effect for the flat window, and El = 14-20° at Az = 145 for the flat window. This research, although limited, showed that VGs might be good candidates to reduce aero-optical effects for missions that require looking into the wake of the turret, and won't be adversely affected by increased $OPD_{RMS}$ for certain side-looking angles, $\alpha < 120°$ for $50° < \beta < 70°$, but additional aero-optical measurements at larger azimuthal angles are needed to fully quantify the range of viewing angles, where VGs have positive mitigation effect. Future work in mitigating aero-optical aberrations with VGs might include performing additional fluidic measurements to fully quantify the effects of the vortices induced by VGs on the varying flow features around the turret. This can be complemented with additional high-fidelity CFD simulations. Also, aero-optical measurements in the forward-looking direction can be performed as well, as it was been postulated that the necklace vortex directly drives observed unsteady defocus on the laser at these angles [16], and the VGs have been shown to modify the necklace vortex and force it away from the turret. A more in-depth study of various VG configurations and sizes could also be performed. Finally, the combination of VGs and other flow control devices, both passive and active can be investigated. The combination of several devices could provide substantial improvement of $OPD_{RMS}$ over a broader range of viewing angles than can be achieved with just a single flow control method.

## Acknowledgments

The authors would like to thank the Northern Air personnel, especially Kevin Tessmer for providing technical assistance during flight tests. We would also like to thank Matthew Krizo from AFIT for providing assistance on the laser tracking system. Finally, the authors would like to thank Grady Graham for his invaluable help in performing CFD simulations for this paper.

These efforts were sponsored by the High Energy Laser Division of the Joint Technology Office (HEL JTO) and supported by the Air Force Office of Scientific Research, Grant number FA9550-07-1-0574. The U.S. Government is authorized to reproduce and distribute reprints for governmental purposes notwithstanding any copyright notation thereon.

**References**

[1] S. Gordeyev and E. Jumper, "Fluid Dynamics and Aero-Optics of Turrets", *Progress in Aerospace Sciences*, **46**, (2010), pp. 388-400.

[2] C. Porter, S. Gordeyev, M. Zenk and E. Jumper, **"**Flight Measurements of the Aero-Optical Environment around a Flat-Windowed Turret", *AIAA Journal*, Vol. **51**, No. 6, Jun. 2013, pp. 1394-1403.

[3] N. De Lucca, S. Gordeyev and E.J. Jumper, **"**In-flight aero-optics of turrets", *Journal of Optical Engineering*, **52**(7), 071405, 2013.

[4] N. De Lucca, S. Gordeyev and E. Jumper, "Comparison of Aero-Optical Measurements from the Flight Test of Full and Hemispherical Turrets on the Airborne Aero-Optics Laboratory", AIAA Paper 2012-2985, 2012.

[5] R. Jelic, S. Sherer and R.Greendyke, "Simulation of Various Turret Configurations at Subsonic and Transonic Flight Conditions Using OVERFLOW", AIAA Paper 2012-464, 2012.

[6] K. Wang, M. Weng, S. Gordeyev and E. Jumper, **"**Computation of Aero-Optical Distortions over a Cylindrical Turret with Passive Flow Control**"**, AIAA Paper 2010-4498, 2010.

[7] M. Weng, A.Mani and S. Gordeyev, "Physics and Computation of Aero-Optics", Annual Review of Fluid Mechanics, Vol. 44, pp. 299-321, 2012.

[8] P.E. Morgan and M.R. Visbal., "Hybrid Reynolds-Averaged Navier-Stokes/Large-Eddy Simulation Investigating Control of Flow over a Turret", *Journal of Aircraft*, **49**(*6*), pp. 1700-1717, 2012.

[9] S. Gordeyev, R. Burns, E. Jumper, S. Gogineni, M. Paul and D.J. Wittich, "Aero-Optical Mitigation of Shocks Around Turrets at Transonic Speeds Using Passive Flow Control", AIAA Paper 2013-0717, 2013.

[10] S.Gordeyev, J. Cress, A. Smith and E. Jumper "Improvement in Optical Environment over Turrets with Flat Window Using Passive Flow Control", AIAA Paper 2010-4492, 2010.

[11] B. Vukasinovic, A. Glezer, S Gordeyev and E. Jumper, "Flow Control for Aero-Optics Application", *Experiments in Fluids*, **54**, p. 1492, 2013.

[12] Wallace, R. "Control of Turbulent Flow Over an Articulating Turret for Reduction of Adverse Aero-Optic Effects", PhD Thesis, Syracuse University, 2011.

[13] E.J. Jumper, M. Zenk, S. Gordeyev, D. Cavalieri and M.R. Whiteley, "Airborne Aero-Optics Laboratory", *Journal of Optical Engineering*, **52**(7), 071408, 2013.

[14] Whiteley, MR, Goorskey DJ, and Drye, R, "Aero-optical jitter estimation using higher-order wavefronts", *Opt. Eng.* **52**(7), 071411, 2013.

[15] S. Gordeyev, J.A. Cress, E. Jumper and A.B. Cain, "Aero-Optical Environment Around a Cylindrical Turret with a Flat Window", *AIAA Journal*, Vol. 49, No. 2, pp. 308-315, 2011.
[16] N. De Lucca, S. Gordeyev, E. Jumper and D.J.Wittich, "Aero-Optical Environment around Turrets at Forward-Viewing Angles", AIAA Paper 2013-0721, 2013.